Engineering Structures 284 (2023) 115993

Contents lists available at ScienceDirect

Engineering Structures

journal homepage: www.elsevier.com/locate/engstruct

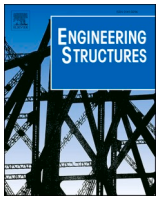

Monitoring the dynamic response of a pedestrian bridge by using low-cost GNSS receivers

Chenyu Xue, Panos A. Psimoulis *

Nottingham Geospatial Institute, The University of Nottingham, Nottingham, UK

ARTICLE INFO

Keywords:
Bridge monitoring
Dynamic response
Multi-GNSS time-series
Low-cost GNSS
Spectral analysis

ABSTRACT

The development of low-cost GNSS receivers with carrier-phase measurement capacity has led to low-budget GNSS applications of higher accuracy and precision. Recent studies have mainly been carried out with those low-cost receivers for landslide monitoring and achieved promising results. In this study, the performance of two closely-spaced high-rate low-cost GNSS receivers was assessed against the robotic total station (RTS) and geodetic GNSS receiver in monitoring the dynamic response of a major pedestrian suspension bridge at the mid-span. Potential accuracy improvement by the combination of two low-cost GNSS time-series was also examined. It was proved that multi-GNSS solution is required to resolve potential outliers and offsets of the low-cost GNSS time-series, due to cycle slip induced errors. The analysis of the low-cost GNSS time-series showed that the low-cost GNSS receivers can estimate (i) the main dominant frequencies of the bridge with the same accuracy as the geodetic-grade GNSS receiver and (ii) the amplitude of the bridge response with difference of ~3 mm with respect the geodetic GNSS receiver due to higher noise level. This study revealed the prospect of utilising low-cost GNSS sensors in monitoring dynamic displacement with frequency of 1–3 Hz, corresponding to relatively rigid structures (e.g., short span bridges, etc.).

1. Introduction

The structural health monitoring (SHM) of civil engineering infrastructure has greatly evolved over the last two decades, especially with the contribution of GNSS technology. The application of GNSS for SHM has frequently been tested and gradually developed, proving to be reliable in monitoring both low-frequency (<1 Hz) [1–4] and high-frequency (>1 Hz) [5–7] displacement motion either in real-time kinematic (RTK) [3,8] or post-processing kinematic (PPK) mode [1,5,6]. Based on experimental studies and practical applications, GPS/GNSS measurements have been proved reliable in monitoring dynamic motion in the range of cm to a few mm [9–12], whereas it can determine the frequency motion accurately for frequencies up to 4–5 Hz [6,7,10].

Despite the development of GNSS technology, to meet the goal in many SHM applications to achieve mm-level accuracy [13,14], the survey-grade GNSS receivers/antennas are conventionally used. However, one of the major drawbacks is their high cost. For instance, GNSS receivers have been adopted in the monitoring system of Tsing Ma Bridge [15] and Forth Road Bridge [8], but the relatively high cost of the geodetic GNSS receivers has limited the number of installed GNSS receivers on the bridges. Consequently, the assessment of the bridge response is based only on few key locations of the bridge (i.e., midspan, pylons).

The recent development of low-cost GNSS receivers broadens their potential in high-precision applications thanks to their capacity for high-frequency sampling rate (up to 10 Hz), multi-GNSS (GPS, GLONASS, Galileo, Beidou, etc.) and precise carrier phase observations. These advancements imply that a more precise positioning with low-cost GNSS receivers could be achievable since the measurement precision is better than ~2 mm with carrier phase observations [16], while the precision for code measurements is at centimetre to decimetre level [17].

Compared to the high-cost survey-grade receivers, these recently emerged low-cost GNSS receiver models are normally small, light, and compact, making them ideal for establishing monitoring networks in challenging environments with instruments facing a high risk of damage or loss. Despite the emergence of dual-frequency low-cost GNSS receivers, the single-frequency low-cost GNSS receivers still dominate the current low-cost GNSS market [18]. The single-frequency low-cost GNSS receivers face problems such as longer ambiguity fixing time and cycle slip susceptibility, and their available functionalities, such as low noise

* Corresponding author at: Nottingham Geospatial Building, The University of Nottingham, Triumph Road, Nottingham NG7 2TU, UK.
E-mail address: panagiotis.psimoulis@nottingham.ac.uk (P.A. Psimoulis).

https://doi.org/10.1016/j.engstruct.2023.115993

Available online 23 March 2023

amplifier (LNA), receiver hardware multipath mitigation, oscillators, etc., leads theoretically to lower quality observables compared to geodetic GNSS receivers. Furthermore, the low-cost patch antennas also have weaker multipath rejection performance than geodetic grade antennas [19], and the accurate calibration of the phase centre from low-cost antennas is usually not conducted.

Although low-cost GNSS measurements are characterised by a comparatively higher noise level, many studies were conducted on geodetic monitoring and precise positioning applications. The positioning accuracy and RTK capability of low-cost GNSS receivers/antennas were evaluated, and it was concluded that the performance of the single-frequency low-cost receiver could be comparable to that of a single-frequency geodetic receiver under certain conditions such as long acquisition time, short baseline length, and use of an external antenna [20–22]. The low-cost receivers were also tested for monitoring slowly developed deformation such as landslides or local monitoring projects [22–24], where the performance of low-cost GNSS receivers was assessed based on controlled experiments by using a geodetic reference station (geodetic receiver/antenna) to ensure high-quality reference observations. Furthermore, experimental studies of the assessment of low-cost GNSS receivers' accuracy in monitoring static, slow-motion [22,25] and dynamic motion [26] have revealed cm to mm-level accuracy of the low-cost receivers and the beneficial contribution of multi-GNSS observations to the accuracy and precision of the GNSS solution. Also, it was shown that the low-cost GNSS solution could be improved by deploying the geodetic antenna instead of the patch antenna at the rover station [22,27], and a geodetic grade antenna at the base station, while the base GNSS receiver type seemed to have a negligible impact on the low-cost GNSS rover station performance [25,26].

Despite the surging trend of research in low-cost GNSS receivers for dynamic deformation monitoring applications, most of the studies were focused on the experimental assessment of dynamic motion monitoring [26,28,29], and only a few studies applied low-cost GNSS receivers in practical SHM cases [30,31]. More specifically, Poluzzi et al. (2020) [30] focused on the analysis of the precision of low-cost GNSS receivers for structural monitoring by investigating different parameters (GNSS data duration, GNSS software), whereas Manzini et al. (2022) [31] investigated the performance of low-cost GNSS receivers in bridge monitoring, limiting though the sampling rate to 1 Hz.

To bridge the gap of low-cost GNSS receivers in SHM of civil engineering structures also focusing on the dynamic response of the structure and frequencies larger than 1 Hz, in this study, we deployed two low-cost GNSS stations on a medium-span suspension bridge to evaluate their performance in monitoring bridge dynamic response against a geodetic GNSS receiver and a Robotic Total Station (RTS). The reliable and mm-level accurate performance of RTS in structural monitoring has been proved in previous experimental studies [9,32], whereas geodetic-grade GNSS receivers have been applied successfully in structural monitoring by improving their performance with adaptation of filtering techniques of GNSS time-series analysis [14] or combination with other sensors (e.g. accelerometers [5], RTS [33]). The main aim of this study is to evaluate how accurate the performance the low-cost GNSS receivers is against RTS, which is considered the ground truth, and whether low-cost GNSS receivers can compete with the geodetic-grade GNSS receivers in structural monitoring. More specifically, we evaluate: (i) the quality of the low-cost GNSS solutions and potential weaknesses, (ii) the accuracy of the low-cost GNSS receiver in determining the major modal frequencies and the amplitude of the dynamic response of the bridge, and (iii) whether the deployment of two closely-spaced GNSS receivers can improve the GNSS solution, a strategy which has been applied in other experimental studies [25,26,28,34].

2. Experimentation

2.1. Experiment design

To assess the feasibility of low-cost GNSS receivers in SHM applications, a monitoring campaign was carried out at Wilford Suspension Bridge, a pedestrian bridge which was extensively used in geodetic and surveying projects of bridge monitoring with well characterised bridge response [5,13,35,36]. A geodetic GNSS receiver and a robotic total station (RTS) were also deployed to record the bridge response continuously and simultaneously to validate the performance of the low-cost GNSS receivers. Based on the mm-level accuracy of the RTS, which was proved in the experimental studies of Psimoulis and Stiros [9,32] and previous RTS bridge monitoring applications [37–40], RTS measurements were used as the ground truth for the response amplitude, while the geodetic GNSS receiver measurements were used as the ground truth for the modal frequencies due to its constant sampling rate and its proven capability for modal frequency derivation of major engineering structures [6].

The bridge midspan was selected as one of the key points of the bridge to be monitored, as it is expected to have a greater response. For a clearer identification of the bridge response, the bridge was excited by designated human-imposed loads of various patterns, such as walking, marching, swinging, jumping etc., to simulate possible loading scenarios on the bridge and to characterise different modal frequencies when the bridge was subjected to vertical, lateral, and torsional displacement.

2.2. Experiment implementation

Wilford Suspension Bridge is a 69-m long suspension pedestrian bridge located in Nottingham. Results from previous studies showed that the main modal frequency of the Wilford bridge is ~1.69 Hz [13], corresponding to the first vertical mode, while the 1st lateral modal and the 2nd vertical frequencies are ~1.44 and ~2.81 Hz, respectively, based on Finite Element Method (FEM) analysis [41]. Those three modal frequencies are the only lower than 5 Hz and could be detected by GNSS measurements, based on the GNSS receivers sampling rate (10 Hz) and Nyquist frequency limitation [6].

In the experiment, several different sensors were deployed along the bridge to monitor the bridge response when it was subjected to different human-induced excitations. The locations of each sensor and corresponding measuring device are illustrated in Figs. 1 and 2 respectively. Four geodetic-grade GNSS stations, were installed on the bridge, two at quarter-spans of the bridge on the south side (location A, D) and two at midspan; one on the north (location B) and one on the south side (location C) of the bridge. The GNSS antennas mounted at the midspan (location B, C) were also integrated with 360° reflective prisms underneath the antenna used as targets for RTS measurement (Fig. 2). Near location B, two closely spaced patch antennas, each connected to low-cost GNSS receiver, were also deployed and orientated to the same azimuth. Both patch antennas were attached to a metal ground plane and clamped firmly to the handrails (Fig. 2). Furthermore, the two patch antennas had an in-between distance of 20 cm to fulfil the requirement of more than half-wavelength of GNSS L1 signal (i.e., L1 carrier wavelength is ~19.0 cm) distance between the two antennas to reduce mutual coupling impact [26,42]. Two raspberry pi 3 models were used for data logging and acquisition for the low-cost GNSS receivers with the help of compiled RTKLIB 'STRSVR' module. Two RTSs and a geodetic-grade GNSS reference station were established at the riverbank, on a stable ground condition, free from vibrations (Fig. 2).

The geodetic-grade GNSS stations used for the experiment were consisted of Leica GS10 receiver and Leica AS10 antenna. Leica GS10 receiver has the capacity to record GPS, GLONASS, Galileo and BeiDou satellite signal, with nominal precision in the horizontal and vertical components of 8 mm ± 1 ppm and 15 mm ± 1 ppm, respectively, for RTK mode [43]. Leica AS10 geodetic antenna has the capacity to receive

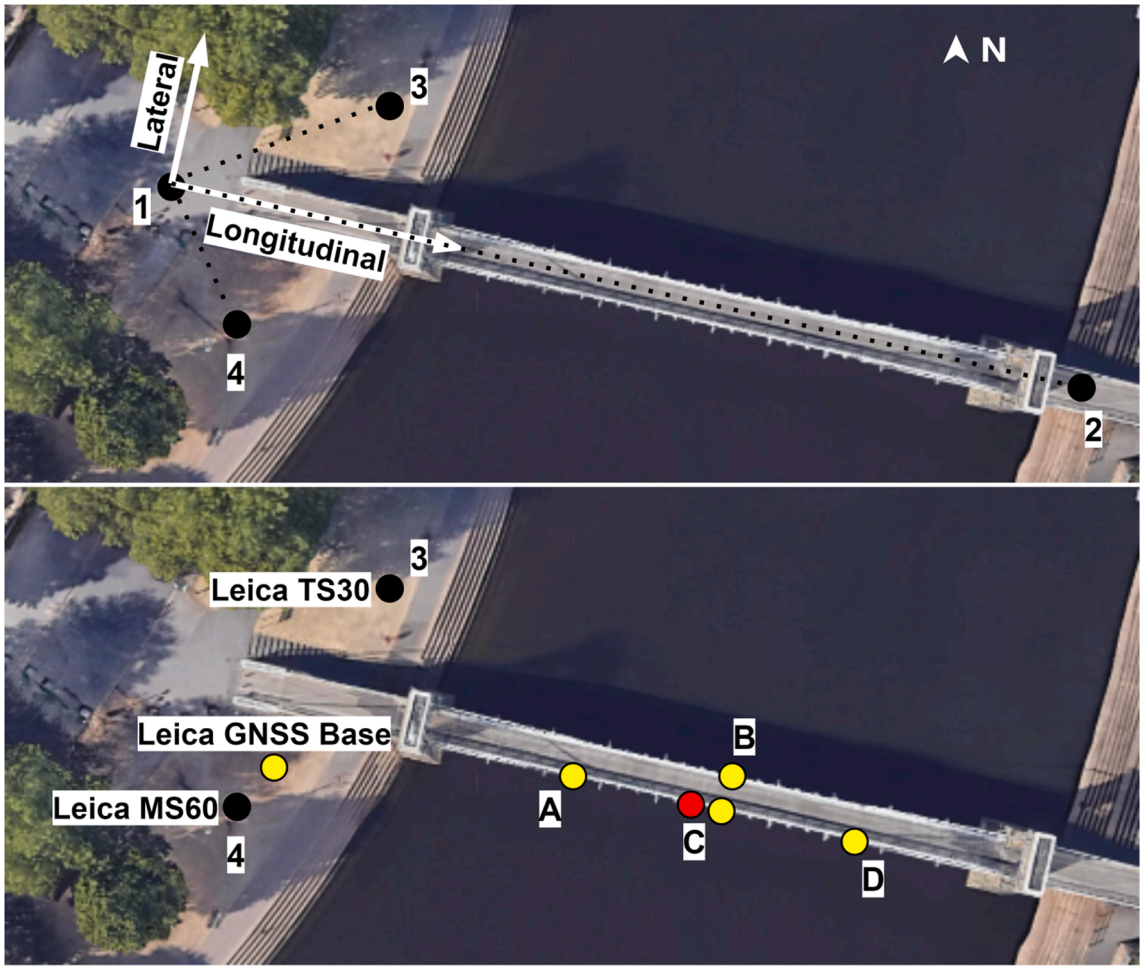

Fig. 1. (top): Wilford pedestrian bridge on River Trent and the location of points 1 and 2 which defined the bridge centreline and points 3 and 4 which were the locations of the two RTSs. (bottom) The location of the geodetic-grade GNSS stations on the bridge (yellow circles), the location of the low-cost GNSS receivers (red circle) and the location of the two RTSs (MS60 and TS30) and the location of the geodetic-grade GNSS base station. (For interpretation of the references to colour in this figure legend, the reader is referred to the web version of this article.)

multi-frequency multi-GNSS signals. The low-cost GNSS receiver used for the experiment was u-blox M8T receiver, which is a single frequency low-cost GNSS receiver with a nominal accuracy of 2.5 m in autonomous mode [44]. The RTS Leica MS60 has nominal precision of 1 mm + 1.5 ppm in the distance and 1'' in the angular measurements [45].

The two RTSs of this study were Leica TS30 and MS60, which were deployed on the north and south of the riverbank from the bridge aiming at the targets located at Locations B and C, respectively. Both RTSs were configured to record the position of the prisms with respect bridge coordinate system with a 10-Hz sampling rate. However, due to the unstable sampling rate of RTS, the actual acquisition frequency is in the range of 5–7 Hz [9,38]. To synchronise the RTS measurements with GNSS time, TS30 was connected to a GNSS antenna forming a GNSS smart station [43]. The coordinate system used for the RTS was preconfigured to the bridge axis, with the x-axis parallel to the longitudinal axis of the bridge and the y-axis parallel to the lateral axis of the bridge. As for GNSS measurements, all GNSS receivers (irrespective of rover and base) recorded GPS and GLONASS observations. The excitations of the bridge were generated by a group of eight people with different loading patterns and activities, summarised in Table 1.

3. Data processing and analysis

The RTS measurements were pre-configured to a local Bridge Coordinate System (BCS). This was achieved, by defining two points, point 1 and 2, on the centreline of the bridge, where the RTS was set up at point 1 and used a prism at point 2 as reference point to determine a local coordinate system with x-axis the longitudinal axis of the bridge. Then, with RTS at Point 1, Points 3 and 4 at the embankment were defined. Finally, two RTSs were set up at the known Points 3 and 4 and oriented to the known Point 1, to determine the coordinate system for the bridge monitoring. Therefore, the RTS time-series would directly reflect the displacements regarding the longitudinal, lateral, and vertical axis of the bridge.

The GNSS measurements were post-processed in RTKLIB to obtain baseline solutions formed between the rover stations (u-blox and Leica) and base station. RTKLIB is free, open-source software for GNSS data processing, which has been tested and applied in several GNSS (geodetic and low-cost) applications [14,25,26]. In this study, an advanced version of RTKLIB developed by Everett [46] (RTKLIB 2.4.3(demo 5)) based on RTKLIB 2.4.3 [47] was used to reduce false fixes and add more constraints for ambiguity resolution enhancement [48]. The GNSS data were processed in kinematic mode adopting standard configuration for short-baseline monitoring applications, i.e., continuous ambiguity resolution, 15° elevation mask, broadcast ephemeris and ionospheric corrections [14,25,26]. A detailed configuration of the GNSS processing can be found in supplementary material Table S1 [49]. The output of RTKLIB processing is the coordinate time-series obtained in a local Easting (E), Northing (N), Up-vertical (U) coordinate system as baseline solutions. To have consistency in RTS/GNSS data comparison, the GNSS

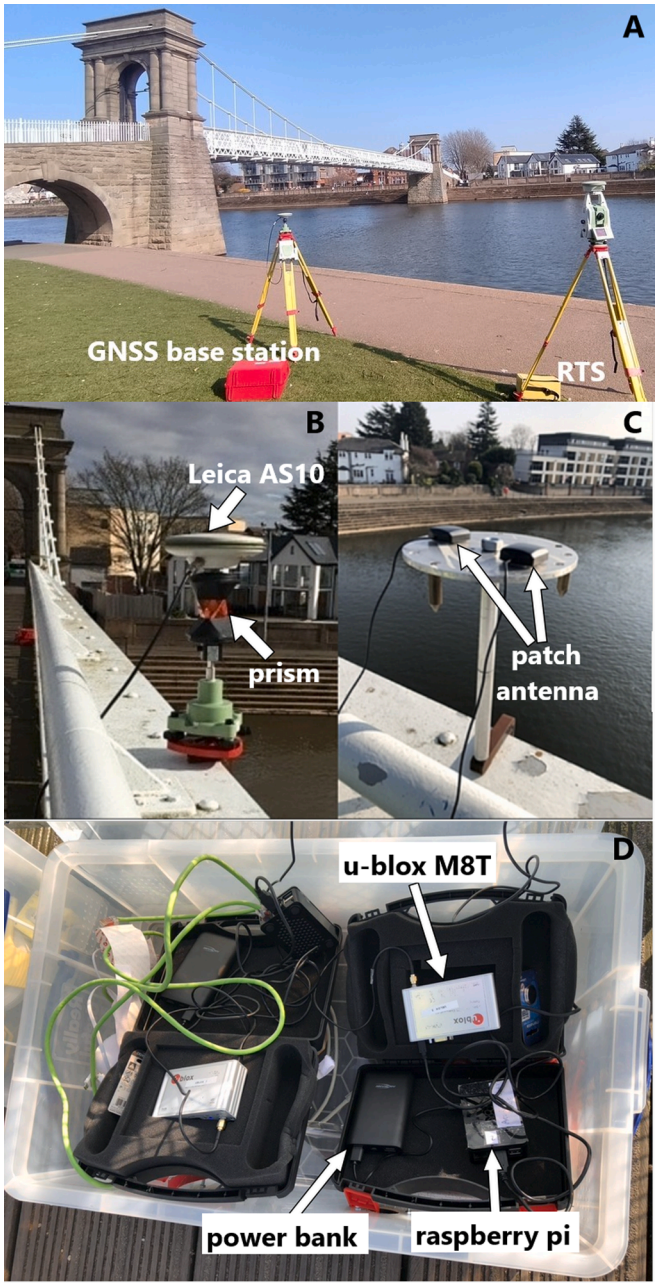

Fig. 2. (a)Top panel: Wilford pedestrian bridge on River Trent and the locations of GNSS base station and RTS on the riverbank; (b) Leica AS10 antenna on the midspan of the bridge (location C) with reflective prisms mounted underneath as the RTS target (c) the two patch antennas on the ground-plane at location C; (d) the two u-blox M8T receivers, with each one connected to the patch antenna and raspberry pi-3, and the latter was powered by power bank.

computed coordinates were transformed to the BCS based on the angle formed by the bridge longitudinal axis with the East-West direction (~12°) via the linear coordinate transformation matrix [9]. Fig. 3 shows the RTS and GNSS (Leica and u-blox receivers) time-series of the representative case of excitation 04 in the bridge coordinate system with respect to the equilibrium point corresponding to the start of the recordings.

The GNSS and RTS time-series were analysed both in the time and frequency domain. The GNSS measurements suffered from low-frequency errors (<0.1 Hz), with the multipath effect being one of the dominant errors in GNSS SHM applications [50–52]. Furthermore, the patch antennas used for the low-cost GNSS measurements were

Table 1
The starting and ending time (unit: s) of different excitation events. The time-stamps for the measurements of all sensors are with respect the starting time of the experiment, coinciding with the logging time of GNSS base station receiver (i.e., 22/03/2019 14:44:30.1000 GPS Time).

Excitation	Start	End	Activity
04	2718	2766	Non-synchronised jump in the bridge midspan
05	2832	2882	Synchronised jump on the north side of the bridge midspan
06	3056	3096	Synchronised jump on the south side of the bridge midspan
07	3237	3285	Synchronised jump with the group spread along the bridge at the bridge midspan
08	3416	3456	Synchronised jump on the north side of the bridge midspan
09	3616	3672	Synchronised swing of the bridge

uncalibrated, which could lead to phase centre variation (PCV) errors. PCV errors depend on the elevation and azimuth of the tracked satellites and the signal frequency, which could generate a low-frequency mm to cm-level error for the horizontal and vertical components, respectively [53].

Therefore, to mitigate the low-frequency errors, including the multipath effect which affects both geodetic and low-cost GNSS time-series, the GNSS time-series of both geodetic and low-cost receivers were filtered by using 8th order Chebyshev high-pass filter with a cut-off frequency of 0.1 Hz and a passband ripple of 1 dB to extract the bridge high-frequency dynamic response from the GNSS time-series [35]. The RTS time-series are not affected by low-frequency errors similar to those of GNSS measurement biases during the bridge monitoring. Hence no filtering was required for the RTS time-series. Fig. 4 shows the GNSS time-series of excitation 04 after the application of the high-pass filter. It is evident that the low-frequency noise of the initial GNSS time-series has been effectively mitigated, and the filtered GNSS time-series express mainly the dynamic response of the bridge.

As aforementioned, RTS measurements are non-equidistant in time due to unstable sampling rate and susceptible to cycle losses in case of high-frequency oscillations [36]. To compare the GNSS time-series against the RTS time-series, the RTS measurement were resampled and linearly interpolated in time to the nearest 0.1 s to synchronise with the GNSS measurement. Then spectral analysis using Discrete Fourier Transform (DFT) was applied for both RTS and GPS time-series, aiming to reveal the frequencies that are present within the time-series, corresponding to the main modal frequencies. Fig. 5 illustrates the spectra of the RTS and GNSS time-series.

To evaluate the performance of the GNSS time-series (Leica GS10 and u-blox) against the RTS time-series, which was considered the truth for the determination of the amplitude of the dynamic response of the bridge, two approaches were adopted: (i) by determining the maximum dynamic displacement using the peak-picking approach of the filtered time-series of GNSS and the initial RTS time-series and (ii) by computing the Moving Root-Mean-Square (MRMS), where the MRMS was expressed by Eq. (1):

$$\mathrm{MRMS} = \sqrt{\frac{1}{j-i+1}\sum_{i}^{j} x_k{}^2} \tag{1}$$

where x_k denotes the measurement from the equilibrium point at epoch k in longitudinal, lateral, and vertical axes, k = I, i + 1, …, j, and j-i + 1 denotes the size of the sliding window.

The MRMS is a similar approach of using the moving standard deviation as an indication of the dynamic response of the bridge [8], since the RMS gives an indication of the displacement magnitude with respect to the equilibrium point where it is assumed to be no displacement. By using the MRMS, the displacement variation can be expressed as a function of time.

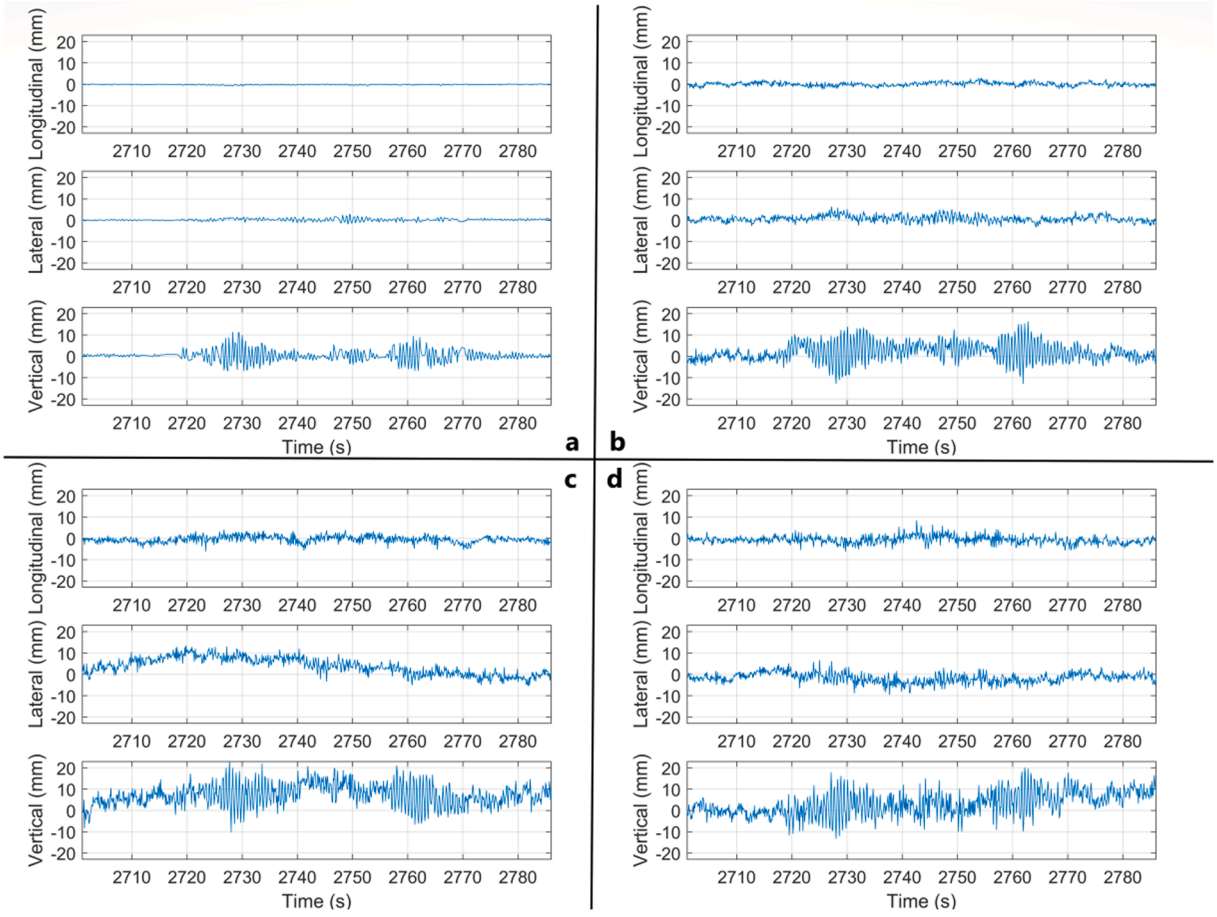

Fig. 3. Initial time-series of (a) RTS, (b) Leica GS 10, (c) u-blox1, and (d) u-blox2 for the longitudinal, lateral and Up-component of excitation 04.

Furthermore, the average combination of two closely-spaced u-blox rover measurements was also evaluated, which was later compared with separate u-blox, Leica, and RTS results to detect any potential accuracy improvement. Both the weighted average and the mean of two low-cost time-series were conducted for the average combination. The weight of the weighted average was calculated based on the estimated standard deviation of the solution obtained from the output from the respective u-blox time-series.

Also, the noise level for each instrument was determined based on ~20–30 s period before the excitation by defining the $\pm 1\sigma$ noise level, where sigma is the standard deviation of measurement for the corresponding period. Finally, to evaluate the measurement difference between the low-cost and geodetic GNSS receivers, the Root Mean Square Error (RMSE)s were calculated between two different time-series using Eq. (2):

$$\mathrm{RMSE} = \sqrt{\frac{\sum_{i=1}^{n}(x_{1,i} - x_{2,i})^2}{n}} \tag{2}$$

where $x_{1,i}$ and $x_{2,i}$ are the respective measurements of two different techniques at epoch *I,* and n is the number of elapsed epochs.

4. Results analysis

4.1. Comparison analysis between GPS-only and multi-GNSS

Considering the relatively challenging observation measurement on the bridge (obstructions, multipath, etc.) and the poor multipath suppressing capability of the patch antenna, the potential beneficial contribution of multi-GNSS observations was examined. The accuracy and availability improvement utilising multi-GNSS solutions has already been proven compared to GPS-only solutions in precise positioning and SHM [14,54,55]. In the current study, it is evaluated the benefits of multi-GNSS solutions for the low-cost GNSS in the case of bridge monitoring.

Fig. 6 shows the Easting, Northing and Up-component of GPS-only time-series for the low-cost GNSS receivers and Leica GNSS receiver, and the corresponding number of satellites and Geometric Dilution of Precision (GDOP). The GDOP is a parameter based on the geometry of the GNSS satellite constellation and expresses its impact on the GNSS solution precision [14,25].

Cycle slips are observed in the low-cost u-blox GPS only time-series, particularly at the beginning of the time-series. In contrast, no cycle slips are detected in the Leica GPS-only solution time-series. The cycle slips in the low-cost GPS-only solution are due to a sudden drop in satellite numbers and/or weakened satellite constellation geometry, as reflected by the increase of GDOP value (Fig. 6). However, cycle slips could still occur in periods which are not related to the number and/or geometry of the satellites, and they are probably due to low satellite(s) signal quality as reflected in the signal-to-noise ratio (SNR; Fig. 7). For instance, for the period of the cycle slips occurring between 1650 and 2300 s, significant SNR fluctuations and reductions are also detected for G32 (Fig. 7). Furthermore, it was observed that excluding G32 satellites reduces the occurrence of cycle slips from 1650 to 2300 s significantly.

On the other hand, the global cycle slips are significantly mitigated by applying the multi-GNSS (GPS + GLONASS) solution for the low-cost GNSS receivers (Fig. 8). However, a short period of cycle slips around 1800 s could still be detected for u-blox 2 (Fig. 8 right panel), probably due to low SNR for the G32 satellite (Fig. 7), which can be resolved by excluding the G32 satellite from the solution. In this study, the multi-

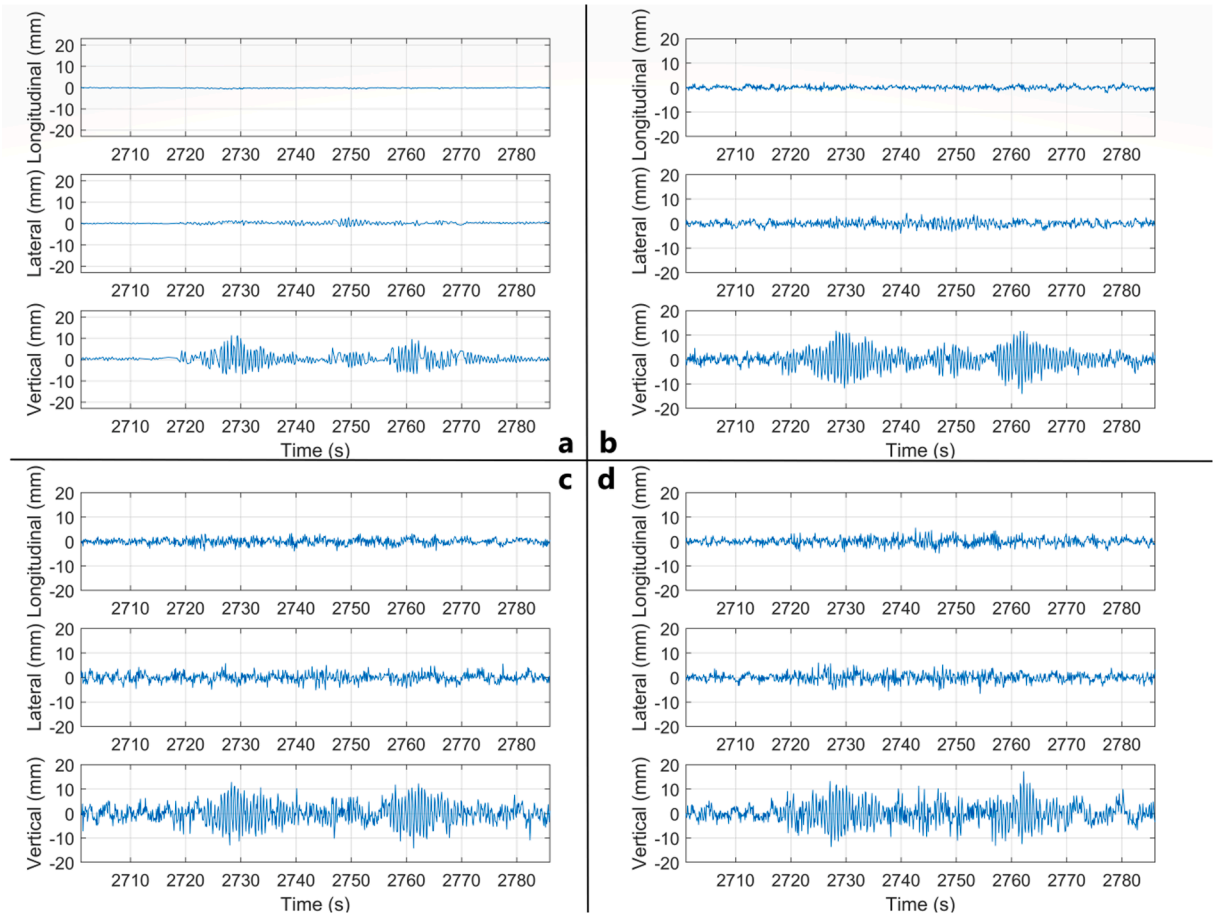

Fig. 4. (a) Time-series of RTS measurements without any filtering and high-pass filtered time-series for (b) Leica GS-10, (c) u-blox1, and (d) u-blox2 for the longitudinal, lateral and Up-component of excitation 04.

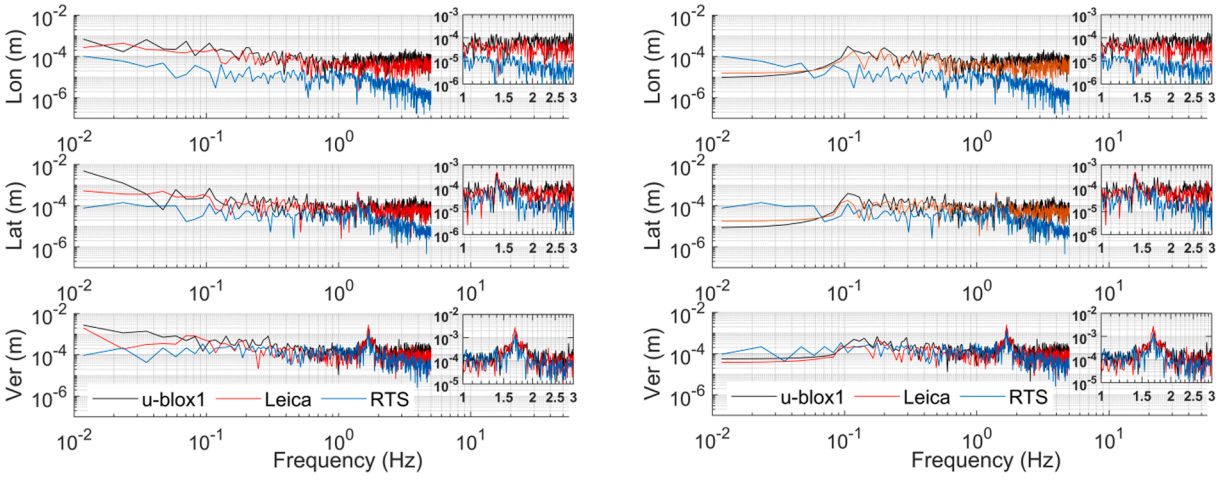

Fig. 5. Spectra of u-blox1, Leica GS10, and RTS (Left) initial time-series and (Right) u-blox1, Leica GS10 high-pass filtered and RTS initial time-series of Longitudinal (top), Lateral (Middle) and Up (Bottom) component of excitation 04 by using DFT analysis, on the top right corner of each figure, a zoomed-in figure for the corresponding spectra is also presented for frequencies from 1 Hz to 3 Hz for a clearer identification of modal frequencies.

GNSS (GPS + GLONASS) solutions were applied for low-cost GNSS receivers and the Leica receiver due to the improved data availability and potential accuracy improvement compared to GPS-only solutions, especially for the low-cost receivers. However, it should be noted that the availability of multi-GNSS satellites (NSAT*) when a 15° elevation mask is applied is quite unstable for the low-cost GNSS solution (Fig. 8) with respect to the same Leica GNSS solution.

4.2. Data analysis – Excitation 04

All RTS/GNSS time-series corresponding to excitations 04–09 were analysed following the same methodology presented in Section 3. The analysis focused on the vertical component, where the main bridge response was expected for all "jumping" excitations (04–08) apart from excitation 09 ("swaying"), where the lateral component was analysed.

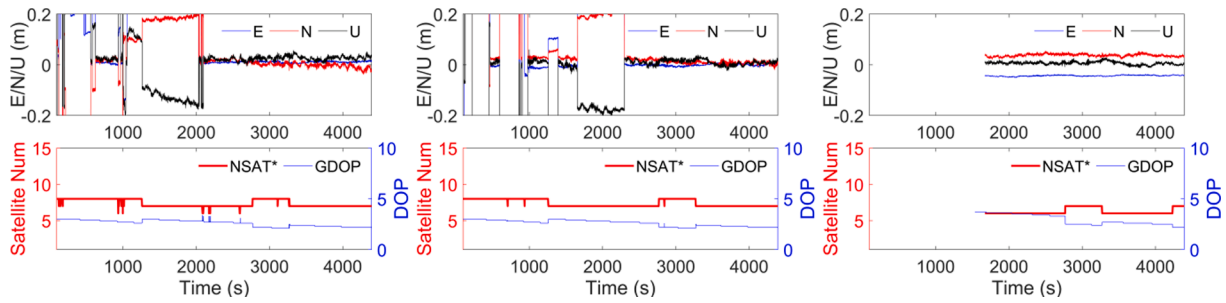

Fig. 6. E/N/U time-series of the GPS-only solution for the three GNSS receivers, (left) u-blox1, (middle) u-blox2 and (right) Leica after the y coordinate are shifted to around zero, and the corresponding number of satellite (NSAT*) and GDOP time-series. The NSAT* expresses the number of available satellites used in coordinate computation when applying the 15° elevation mask. The occurrence of cycle slips can be clearly identified in the two low-cost GNSS receivers from the beginning of the record until 2300 s, whereas the Leica GPS-only solution is not affected by cycle slips. The missing data prior to around 1700 s is due to the delayed Leica GNSS measurement.

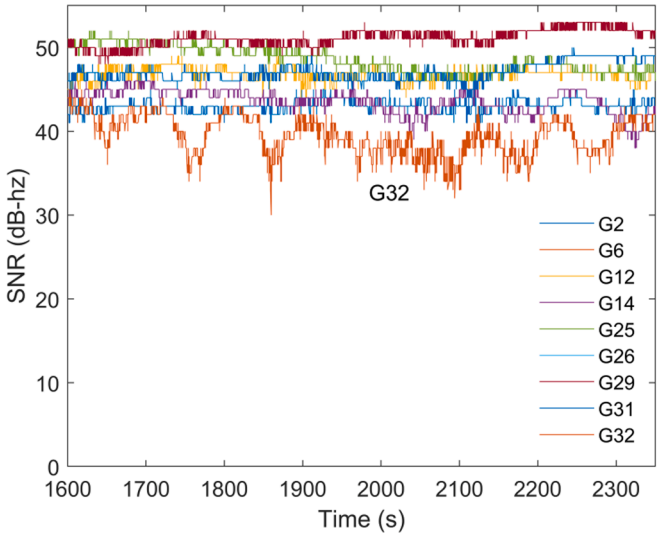

Fig. 7. Signal to Noise Ratio (SNR) of GPS satellites from 1600 s to 2350 s, from Fig. 6 middle panel, it could be seen that cycle slips occur during the period from 1650 s to 2300 s were probably due to the reduction of SNRs of G32 during that period.

The RTS time-series and the high-frequency (10 Hz) GNSS time-series were analysed for the estimation of the response amplitude and the modal frequencies. For every time-series, a period of ~30 s before and after excitation was included, which was considered as the period of relatively stable state of bridge response for evaluating the noise level of the time-series. In the following demonstration, the RTS and GNSS time-series of excitation 04 are used as a representative case of the data analysis and results.

From the initial time-series of excitation 04 (Fig. 3) and the corresponding spectra (Fig. 5), it can be seen that the original RTS time-series has a relatively low noise level compared to the GNSS measurement. In contrast, a clear trend of long-period noise is shown in the GNSS time-series for Leica and low-cost GNSS receivers. The relatively low noise of the RTS time-series is also evident in the spectrum where the low-frequency noise, mainly for frequencies lower than 0.1 Hz, is at a level of $\sim 10^{-4}$ m, whereas the long-period noise of GNSS time-series is of one order higher than RTS (i.e., 10^{-3} m) probably due to the multipath bias, phase centre variation, etc. The relative higher noise level of the GNSS time-series is more evident on the longitudinal axis where no excitation occurred, with a higher noise level also at the band of higher frequency (i.e., >2 Hz). It should also be noted that the u-blox GNSS spectra indicate slightly higher noise but of the same order as the Leica GNSS spectra.

After the application of high-pass filtering, the noise level of the RTS/GNSS time-series was evaluated based on the 1-σ (σ denotes the standard deviation) prior to the excitation (Table 2). For excitation 04 vertical components, the 1-σ is 0.3 mm, 1.4 mm, 2.3 mm and 2.1 mm for RTS, Leica GNSS, u-blox1 and u-blox 2, respectively. It is evident that after filtering the GNSS time-series, they are still of one order higher than the noise of RTS and that u-blox receivers' noise is slightly higher than Leica GNSS receivers. Regarding the response amplitude during the excitation period, it is evident that the dynamic response is reflected in all time-series, with the GNSS time-series having slightly higher amplitude potentially due to the impact of the GNSS measurements noise. More specifically, the peak amplitude during the excitation period is 9.8 mm,

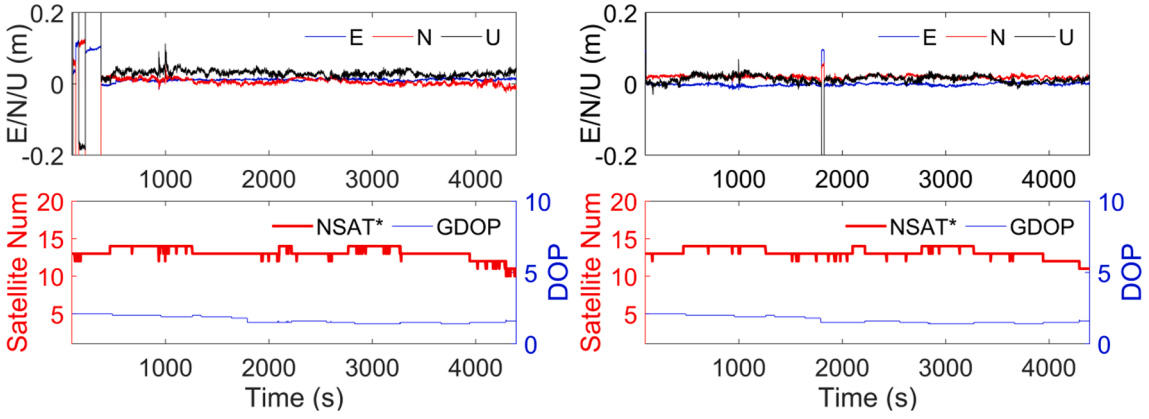

Fig. 8. Same as Fig. 6, for the multi-GNSS (GPS + GLONASS) solution of the low-cost (Left) u-blox1 and (Right) u-blox2 receivers. The occurrence of cycle slips has been mitigated significantly.

Table 2
The standard deviation σ for the high-pass filtered vertical time-series of the 20-s period before excitation for excitations 04–09 (unit: mm).

Excitation	RTS	Leica	U-blox1	U-blox2	(Weighted) Ave
04	0.3	1.4	2.3	2.1	1.8
05	0.2	1.8	2.7	2.6	2.2
06	0.1	1.3	1.4	1.5	1.2
07	0.8	1.6	2.2	1.7	1.7
08	0.3	1.2	1.2	1.1	1.0
09	0.1	1.3	1.7	1.8	1.3

11.4 mm, 13.8 mm and 13.4 mm for RTS, Leica GNSS, u-blox1 and u-blox2, respectively (Fig. 4). Furthermore, the spectra of the filtered GNSS time-series are characterised by limited noise levels, and the main peak of RTS and GNSS (Leica and u-blox) spectra are in agreement with each other, indicating the frequency of 1.680 Hz, as the dominant frequency of the vertical response.

Following the same procedure, the averaged u-blox1 and u-blox2 time-series were also analysed both in the time and frequency domain. It is noticed that the weights, which ranged between 0.45 and 0.55, used in the weighted average have negligible impact on the solution and would result in a similar time-series as simply averaging. From the combination u-blox1 and u-blox2 time-series, it is clear that the derived time-series lies between the u-blox1 and u-blox2 time-series limiting the main errors of the two u-blox time-series. The 1-σ noise level prior to the excitation for the combined u-blox time-series is 1.8 mm, smaller than the corresponding values of the two individual u-blox receivers, while the peak amplitude of the combined u-blox time-series is 13.5 mm, closer to the smaller value (and probably less noisy) of the two u-blox receivers time-series (Fig. 9). The spectra of the averaged time-series were compared to separate low-cost results (Fig. 9). An improvement in the high-frequency band (larger than 1 Hz) is shown by averaging separate solutions, which implies the random errors (white noise) are mitigated by averaging.

The next step of RTS/GNSS data analysis was to calculate the MRMS of the corresponding time-series and analyse the consistency of the GNSS against the RTS, with the RTS being considered the most accurate. The moving window of the MRMS was selected as 5 s, corresponding to 50 samples (epochs) for GNSS data. Fig. 10 shows the RTS and GNSS time-series of the vertical component, the corresponding MRMS, and the ratio of the MRMS of the GNSS estimated MRMS to the RTS estimated MRMS.

Based on the MRMS time-series, it is obvious that the MRMS value of the RTS time-series follows the pattern of excitation. The MRMS starts increasing at t = 2720 s and reaches peak values three times (i.e., 4.9 mm at ~2729 s, 2.1 mm at ~2749 s and 4.0 mm at 2760 s) until the excitation stops (i.e., t = ~2780 s). The MRMSs of the GNSS time-series follow the same trend as the RTS MRMSs but have higher values, indicating that the GNSS time-series are consistent with the RTS observation, but the higher noise level of the GNSS time-series results in a larger amplitude of the bridge response and consequently higher MRMS values. Furthermore, the MRMSs of the two u-blox time-series have slightly larger values than the MRMSs of the Leica GNSS time-series, especially for the period prior to and after the excitation.

By analysing the ratio of the MRMS GNSS time-series to the MRMS of the RTS time-series, it is obvious that prior to the excitation, the ratio ranges between 2.5 and 11, with the ratio of Leica GNSS time-series having the lower values (ranging between 2.5 and 6), proving the higher noise level of u-blox time-series compared to Leica GNSS time-series. Furthermore, the averaged u-blox ratio time-series has the lowest value among u-blox time-series indicating increased accuracy by averaging operation. In general, during the excitation period, the ratio of the MRMS is reduced significantly, ranging between 1 and 2. The only period during the excitation where the ratios exceed the value of 2 is between t = 2741 s and t = 2746 s when the excitation was temporarily paused. For the period after t = 2775 s, the ratios are increased again, coinciding with the period when the excitation has stopped and the response of the bridge is attenuating. The ratios of the MRMS of low-cost GNSS to RTS are significantly reduced during the excitation period, which is because of the stronger GNSS displacement signal relative to the GNSS noise level. This characteristic has also been used for GNSS deformation monitoring, such as seismic motion [56].

4.3. Data analysis from other excitations

All excitations were analysed following the same methodology as for excitation 04 to analyse the accuracy and performance of u-blox GNSS receivers with respect to Leica GNSS receiver and RTS. More specifically, it was computed: (i) the 1-σ of the RTS/GNSS time-series of the 20-s period prior to the excitations as an indication of the noise level of each time-series, (ii) the peak amplitude of the RTS/GNSS time-series during the excitation, (iii) the MRMS of RTS/GNSS and the corresponding peak value during the excitation, iv) RMSE between u-blox and Leica GNSS receivers and v) the main frequencies as revealed from the spectral analysis of RTS/GNSS time-series.

Table 2 also presents the noise level of the RTS/GNSS time-series based on the 1-σ computation of the time-series corresponding to the period 20-s prior to the excitation for other excitations. It is observed that the lowest noise level is for RTS measurement, whereas the highest noise level is for one of the low-cost u-blox receivers. However, for most

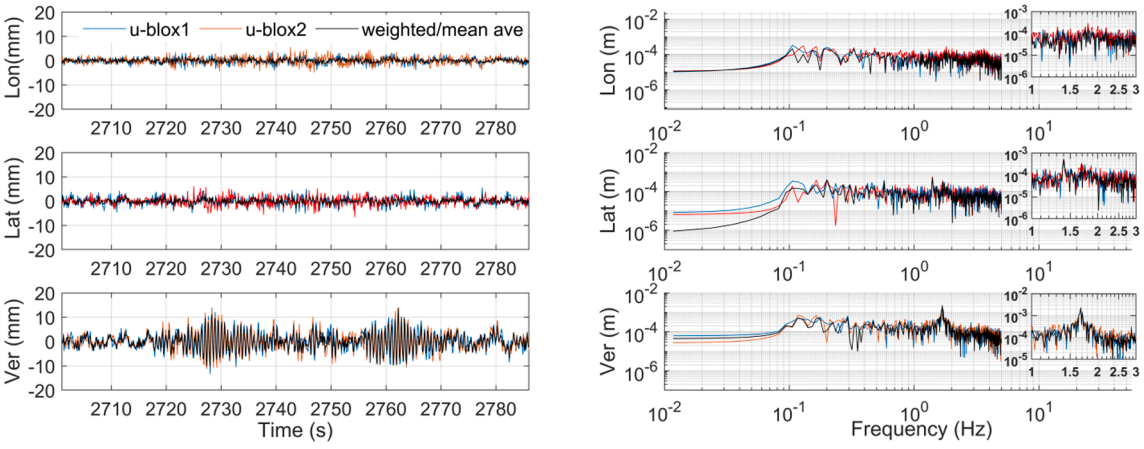

Fig. 9. Comparison between (Left) u-blox1, u-blox 2, and the high-pass filtered averaged time-series and (Right) corresponding DFT spectra for Lon/Lat/ Up for excitation 04, on the top right corner of the spectra figure, a zoomed-in figure for frequencies from 1 Hz to 3 Hz were presented for a clearer identification of modal frequencies.

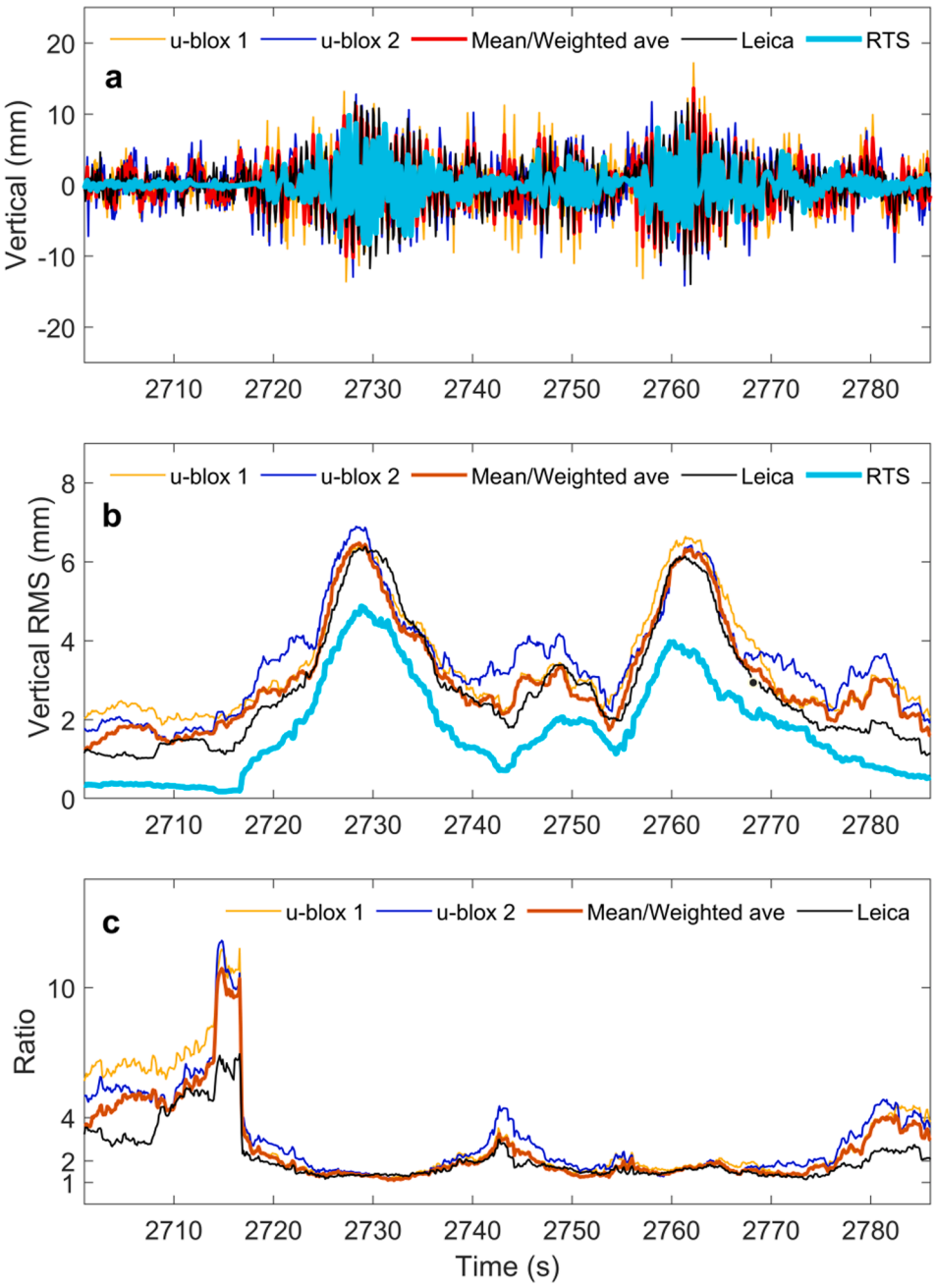

Fig. 10. (a) Vertical time-series of u-blox1, u-blox2, mean/weighted average, Leica, RTS time-series after high-pass filtering for excitation 04, (b) Corresponding MRMS (5 s moving window) for the vertical components of the panel a; (b) Ratio calculated using MRMS from u-blox1, u-blox2, mean/weighted average, Leica with reference to RTS results.

of the excitations (e.g., 06–09), the difference between the noise level of u-blox and Leica GNSS is <0.6 mm. Furthermore, the combined averaging u-blox solution reduces the noise level of the u-blox time-series even lower than that of the Leica GNSS time-series (i.e., excitations 06 and 08), reaching even 1 mm-level.

Then, based on the analysis of the RTS time-series and GNSS high-pass filtered time-series, Table 3 presents the peak amplitude and the peak-MRMS derived from the time-series for each excitation 04–09 of the corresponding excitation period. It is shown that the peak amplitudes derived from the Leica GNSS time-series are normally within 2.6 mm from that of RTS for each excitation. Regarding the u-blox GNSS time-series, their difference of peak-amplitude from the corresponding RTS ranges from 0.2 to 9 mm depending on the u-blox receiver and the excitation. However, the combined averaging u-blox time-series mitigates the error of the least accurate u-blox time-series and limits the deviation of the peak amplitude up to 4.7 mm. Likewise, the peak MRMS of Leica and u-blox GNSS receivers vary about 0.9–2.3 mm and 0.9–3.3 mm from the RTS value, respectively. The MRMSs of Leica GNSS and u-blox GNSS are within 1.9 mm difference. The averaging combined u-blox solution are even in closer proximity to the Leica GNSS results, with the deviation not exceeding 0.6 mm.

Based on Table 3, due to discrepancies in one of the two u-blox GNSS time-series, some relatively large differences between the peak amplitude and MRMS of the two u-blox GNSS receivers were observed. More specifically, for excitation 05, 06 and 07, larger amplitude discrepancies from two u-blox could be seen (with a range of differences between 4.3 and 6 mm) than that of other excitations (with a range of 0.4–2.7 mm) (Table 3). The reason was further investigated in Fig. 11, where it can be

Table 3
Vertical displacement amplitude determined by maximum peak picking from (i) high-pass filtered time-series, and (ii) corresponding MRMS of (i) expressed in parenthesis, with respect to equilibrium point for Excitation 04–09 (unit: mm).

Excitation	RTS	Leica	U-blox1	U-blox2	(Weighted) Ave
04	9.8 (4.9)	11.4 (6.3)	13.8 (6.4)	13.4 (6.9)	13.5 (6.4)
05	6.3 (3.6)	8.9 (4.5)	8.8 (4.5)	13.2 (5.5)	10.5 (4.6)
06	12.5 (5.1)	14.5 (7.4)	9.5 (6.3)	13.8 (7.8)	14.5 (6.9)
07	7.4 (3.1)	7.9 (4.5)	16.5 (5.5)	10.5 (4.5)	12.1 (4.8)
08	10.0 (4.1)	10.0 (5.8)	10.2 (5.6)	11.0 (6.0)	10.6 (5.7)
09	8.8 (4.0)	9.1 (5.4)	10.3 (5.3)	13.0 (7.3)	10.4 (6.0)

seen that for both excitation 05 and 07, a small transient spike occurs in the time-series during the excitation period (around 2840 s for excitation 05 and around 3268 s and 3270 s for excitation 07), which could correlate to the number of satellite variations. As a result, such transient jumps, probably due to receiver hardware, would finally degrade amplitude determination. However, such discrepancies could be mitigated based on the combined averaging of the two u-blox GNSS time-series.

To evaluate the performance difference between low-cost GNSS and geodetic GNSS measurements, the RMSE is adopted for the 20 s before and during excitation. As is shown in Table 4, the maximum RMSE between geodetic GNSS and low-cost GNSS measurement is observed for the excitation period with an average value of 2.5 mm, while for the period prior to the excitation, the RMSE is about 2 mm. In any case, the RMSE of the two u-blox GNSS receivers does not exceed 3.2 mm. Moreover, with the average combination, the RMSEs are further reduced to about 1.7 mm and 2 mm for the period before and during excitation respectively. The latter confirms the overall accuracy improvement by mean/weighted averaging of the two low-cost u-blox GNSS receivers' time-series.

Finally, the modal frequencies derived from the spectral analysis of the RTS and GNSS time-series are presented in Table 5. More specifically, the main modal frequencies derived from the lateral (excitation 09) and the vertical (excitations 04–08) excitations of the bridge are presented. In general, within the same excitation, the modal frequencies detected from RTS and Leica measurement could also be detected from u-blox measurement with a maximum discrepancy of ~0.02 Hz. The frequencies derived from the spectra of both u-blox1 and u-blox2 time-series were in agreement, with some slight deviations (~0.02 Hz) for excitations 06 and 09. Furthermore, the derived frequency from the averaged u-blox time-series were also in close agreement with each low-cost GNSS result.

For the vertical excitations, the main modal frequency was determined in the range of 1.67–1.68 Hz by all instruments (RTS, GNSS Leica and u-blox), also confirming the results from the previous studies [13,35,36]. However, there is a second modal frequency ranging between 2.840 and 2.860 Hz, which corresponds to the first torsional modal frequency produced by the non-synchronised vertical excitation across the width of the bridge in some of the excitations. This frequency was also observed in previous studies [35]. However, it could not be picked up by the RTS time-series due to the relatively low real sampling rate of the RTS (i.e., 5–7 Hz), resulting in a Nyquist frequency of about 3 Hz, which is very close to the targeted modal frequency.

For the lateral excitation (i.e., 09) produced by swaying, the first lateral modal frequency of 1.394 Hz was revealed and confirmed by all the time-series (RTS, Leica and u-blox GNSS), which proves that the u-blox GNSS receivers also perform well to identify the dynamic motion of the horizontal components. The second frequency of 0.801 Hz probably corresponds to the excitation frequency of the swaying-type motion of the group of people. The presence of the excitation frequency in the spectra has also been observed in previous bridge monitoring studies [38].

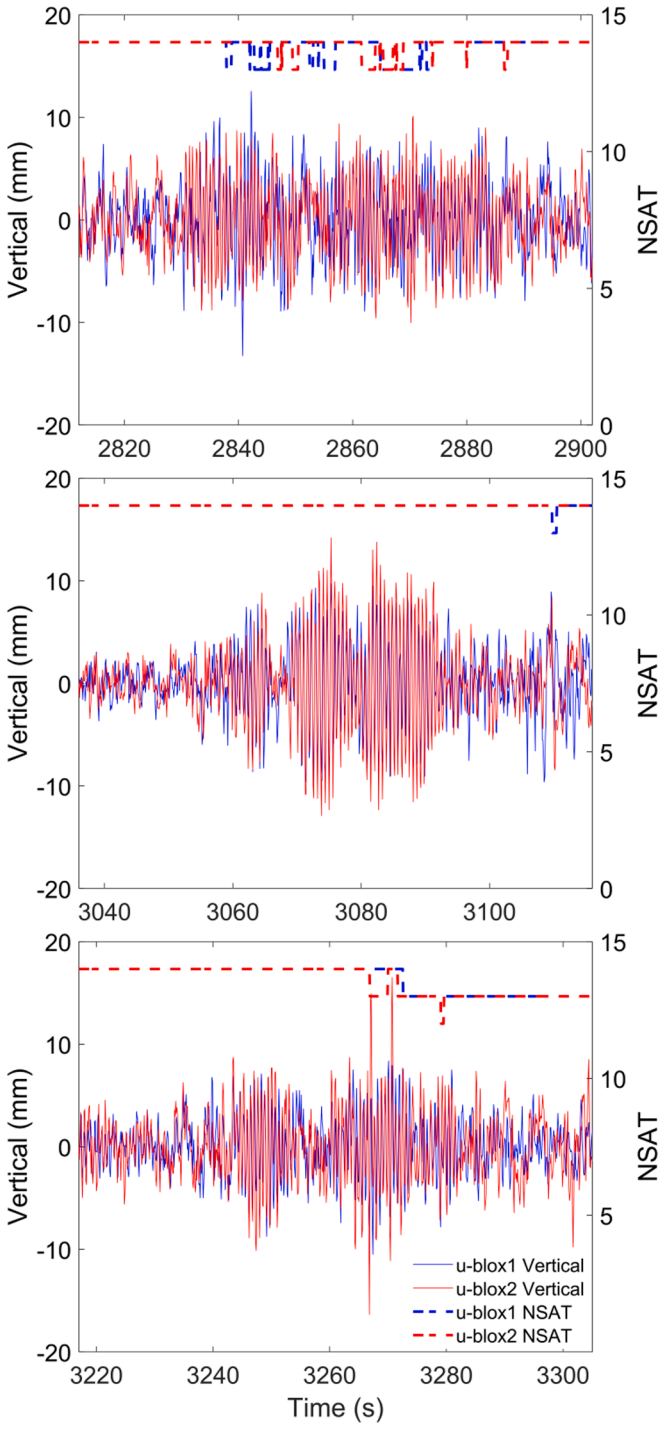

Fig. 11. Occurrence of unexpected spikes in correlation to satellite number drop, u-blox1 Vertical and NSAT time-series (Blue) and u-blox2 Vertical and NSAT time-series (Red) for (Top) excitation 05, (Middle) excitation 06, and (Bottom) excitation 07, where large amplitude deviation between u-blox1 and u-blox2 is identified. (For interpretation of the references to colour in this figure legend, the reader is referred to the web version of this article.)

5. Discussion

From the analysis of the u-blox GNSS time-series and comparison

Table 4
RMSE value (unit: mm) for u-blox1, u-blox2, and mean/weighted averaged u-blox time-series with respect to Leica time-series for the 20-s period prior to the excitation and the period during excitation.

Excitation	u-blox1		u-blox2		Mean/weighted average	
	Before	During	Before	During	Before	During
04	2.2	2.4	2.2	2.9	1.9	2.1
05	3.1	2.9	2.5	3.2	2.4	2.4
06	1.8	2.6	1.6	2.3	1.5	2.0
07	2.2	3.0	1.9	2.6	1.8	2.4
08	1.4	1.7	1.2	1.5	1.2	1.4
09	1.9	2.5	2.1	2.7	1.6	2.2

Table 5
Frequency (unit: Hz) detected from DFT spectral analysis from excitation event 04–09 (Lat: Lateral, Ver: Vertical).

Excitation	Axis	RTS	Leica	u-blox1	u-blox2
04	Ver	1.680	1.680	1.680	1.680
05	Ver	1.676	1.676	1.676	1.676
06	Ver	1.685	1.673/2.846	1.673/2.846	1.685/2.846
07	Ver	1.657	1.646/2.860	1.646/2.838	1.646/2.826
08	Ver	1.673	1.673/2.859	1.673/2.859	1.673/2.859
09	Lat	0.801/1.394	0.801/1.394	0.801/1.394	0.801/1.415

against the performance of geodetic-grade GNSS receiver (i.e., Leica GNSS receiver) and the more reliable RTS measurements, some key points were identified in the performance of u-blox GNSS receivers.

Firstly, it was observed that multiple cycle slips occurred at the beginning of GNSS u-blox observations or after a sudden change of the measuring conditions (see the time interval between 1650 s and 2300 s of Fig. 6 left and middle panel), such as (i) variation of the satellite number, (ii) the quality of satellite signal in one of the satellites (reflected in SNR) and (iii) the change of satellite geometry (reflected by DOP). The cycle slips were more evident for the case of GPS-only solution. Once a second satellite system was applied, leading to multi-GNSS solution (in this study GPS + GLONASS), the cycle slips were reduced significantly.

Then, based on the multi-GNSS solution, the accuracy of the low-cost GNSS receivers in estimating the amplitude and frequency of the bridge response was assessed. The noise level of the high-passed filtered low-cost GNSS time-series was between 1.1 and 2.7 mm, slightly larger than the noise level of the geodetic GNSS time-series and one scale larger than the RTS noise level (Table 2). The estimated peak amplitude using the low-cost GNSS time-series is usually larger than that of the RTS and geodetic GNSS time-series due to higher noise level, with the difference varying from 0.2 mm to 9 mm for the case of RTS (Table 3). However, the estimated MRMS differences between the low-cost GNSS and RTS, and between the geodetic GNSS and RTS, are about 0.9–3.3 mm and 0.9–2.3 mm, respectively. It indicates that there is a greater impact of low-cost receiver noise on the amplitude estimation when a single sample (peak-picking approach) is being used. In contrast, by using MRMS for amplitude estimation this effect is mitigated. Furthermore, the low-cost GNSS noise seems to have a smaller impact for excitations with large amplitude response since the noise level is proportionally smaller than the displacement signal, as reflected in Fig. 10c.

Regarding the estimation of the modal frequency(ies), the low-cost GNSS time-series proved to be as reliable and accurate as the geodetic GNSS time-series, which was also proved in previous experimental studies [26,28]. The performance seemed not to be affected by different modes (lateral or vertical) and the difference between the estimated modal frequency of low-cost GNSS receivers and geodetic GNSS receivers did not exceed 0.03 Hz. The larger differences in modal frequencies seem to occur mainly for the higher modal frequencies potentially due to the relatively higher noise level of the low-cost GNSS data with respect to the response amplitude of the corresponding mode [6]. Moreover, the low-cost GNSS receivers proved to be more suitable than RTS in estimating frequencies higher than 2.5 Hz due to the higher sampling rate, which has also been proved for GNSS time-series in previous studies [33,57].

Finally, the average combination of the two closely-spaced low-cost GNSS receivers' time-series, led to time-series of a lower noise level, which is even lower than that of the geodetic GNSS results for some excitations. In the estimation of the response amplitude (Table 3), the least accurate result from one of the u-blox was also effectively corrected with the average combination, which increased the robustness of the amplitude estimation.

6. Concluding remarks

In this paper, we presented the first study of the application of low-cost consumer-grade GNSS receivers in a short-medium span bridge SHM. The performance of low-cost GNSS receivers was analysed against a geodetic GNSS receiver and RTS in estimating the bridge response characteristics (amplitude and modal frequency).

Two main weaknesses of the low-cost single-frequency GNSS receiver measurements were faced in the challenging application of bridge monitoring. The first weakness was the susceptibility of the single-frequency low-cost GNSS receivers to cycle slips, especially when the single GPS satellite constellation was used, whichwas effectively mitigated by applying multi-GNSS (GPS + GLONASS) solution. The second weakness was the relatively higher noise level of the low-cost GNSS time-series compared to the geodetic GNSS time-series, due to the higher susceptibility of the low-cost GNSS antennas to multipath effect and the higher noise level of the low-cost single-frequency GNSS receivers. In this regard, the approaches of filtering the lower frequency components (<0.1 Hz) of the low-cost GNSS time-series, which is a common approach even for geodetic GNSS time-series, and the combination of two low-cost GNSS receivers were used, to significantly limit the noise level of the low-cost GNSS time-series. Overall, the noise level of the low-cost GNSS receivers introduced an error of 2–3 mm to the estimated bridge response, with respect to the geodetic GNSS time-series, However, the low-cost GNSS time-series proved to be equally accurate to the geodetic GNSS time-series for the determination of the modal frequencies, for a range between 1.5 and 3 Hz.

Hence, the first study of the application of low-cost GNSS receivers in structural monitoring led to promising results indicating that they can be comparable with the geodetic-grade GNSS receivers. Although recent developments of low-cost GNSS receivers have equipped them with dual-frequency GNSS observation capability and potentially more reliable performance [58]. future studies need to shed more light on how to limit the main weaknesses of low-cost GNSS stations even further, such as the impact of low-cost GNSS antennas (multipath effect susceptibility, antenna phase centre calibration) and the higher noise level of low-cost GNSS receivers.

Declaration of Competing Interest

The authors declare that they have no known competing financial interests or personal relationships that could have appeared to influence the work reported in this paper.

Data availability

Data will be made available on request.

Acknowledgement

The authors are grateful for the contribution of Mr. Sean Ince and the participation of the MSc students in the field measurements at Wilford Suspension Bridge.

Funding sources

This research did not receive any specific grant from funding agencies in the public, commercial, or not-for-profit sectors.

Appendix A. Supplementary material

Supplementary data to this article can be found online at 10.1016/j.engstruct.2023.115993.

References

[1] Lovse J, Teskey W, Lachapelle G, Cannon M. Dynamic Deformation Monitoring of Tall Structure Using GPS Technology. J Surv Eng 1995;121(1):35–40. https://doi.org/10.1061/(asce)0733-9453(1995)121:1(35).
[2] Nakamura S. GPS Measurement of Wind-Induced Suspension Bridge Girder Displacements. J Struct Eng 2000;126(12):1413–9. https://doi.org/10.1061/(asce)0733-9445(2000)126:12(1413).
[3] Tamura Y, Matsui M, Pagnini L, Ishibashi R, Yoshida A. Measurement of wind-induced response of buildings using RTK-GPS. J Wind Eng Ind Aerodyn 2002;90(12–15):1783–93. https://doi.org/10.1016/s0167-6105(02)00287-8.
[4] Çelebi M, Sanli A. GPS in Pioneering Dynamic Monitoring of Long-Period Structures. Earthq Spectra 2002;18(1):47–61. https://doi.org/10.1193/1.1461375.
[5] Meng X, Dodson A, Roberts G. Detecting bridge dynamics with GPS and triaxial accelerometers. Eng Struct 2007;29(11):3178–84. https://doi.org/10.1016/j.engstruct.2007.03.012.
[6] Psimoulis P, Pytharouli S, Karambalis D, Stiros S. Potential of Global Positioning System (GPS) to measure frequencies of oscillations of engineering structures. J Sound Vib 2008;318(3):606–23. https://doi.org/10.1016/j.jsv.2008.04.036.
[7] Yi T, Li H, Gu M. Experimental assessment of high-rate GPS receivers for deformation monitoring of bridge. Measurement 2013;46(1):420–32. https://doi.org/10.1016/j.measurement.2012.07.018.
[8] Meng X, Nguyen D, Xie Y, et al. Design and Implementation of a New System for Large Bridge Monitoring—GeoSHM. Sensors 2018;18(3):775. https://doi.org/10.3390/s18030775.
[9] Psimoulis P, Stiros S. Experimental Assessment of the Accuracy of GPS and RTS for the Determination of the Parameters of Oscillation of Major Structures. Comput-Aided Civ Infrastruct Eng 2008;23(5):389–403. https://doi.org/10.1111/j.1467-8667.2008.00547.x.
[10] Moschas F, Stiros S. Measurement of the dynamic displacements and of the modal frequencies of a short-span pedestrian bridge using GPS and an accelerometer. Eng Struct 2011;33(1):10–7. https://doi.org/10.1016/j.engstruct.2010.09.013.
[11] Häberling S, Rothacher M, Zhang Y, Clinton J, Geiger A. Assessment of high-rate GPS using a single-axis shake table. J Geod 2015;89(7):697–709. https://doi.org/10.1007/s00190-015-0808-2.
[12] Psimoulis P, Houlié N, Habboub M, Michel C, Rothacher M. Detection of ground motions using high-rate GPS time-series. Geophys J Int 2018;214(2):1237–51. https://doi.org/10.1093/gji/ggy198.
[13] Yu J, Meng X, Shao X, Yan B, Yang L. Identification of dynamic displacements and modal frequencies of a medium-span suspension bridge using multimode GNSS processing. Eng Struct 2014;81:432–43. https://doi.org/10.1016/j.engstruct.2014.10.010.
[14] Msaewe H, Psimoulis P, Hancock C, Roberts G, Bonenberg L. Monitoring the response of Severn Suspension Bridge in the United Kingdom using multi-GNSS measurements. Struct Control Health Monit 2021;28(11). https://doi.org/10.1002/stc.2830.
[15] Wong K. Instrumentation and health monitoring of cable-supported bridges. Struct Control Health Monit 2004;11(2):91–124. https://doi.org/10.1002/stc.33.
[16] Geng J, Bock Y. Triple-frequency GPS precise point positioning with rapid ambiguity resolution. J Geod 2013;87(5):449–60. https://doi.org/10.1007/s00190-013-0619-2.
[17] Bona P. Precision, Cross Correlation, and Time Correlation of GPS Phase and Code Observations. GPS Solutions 2000;4(2):3–13. https://doi.org/10.1007/pl00012839.
[18] Nie Z, Liu F, Gao Y. Real-time precise point positioning with a low-cost dual-frequency GNSS device. GPS Solutions 2019;24(1). https://doi.org/10.1007/s10291-019-0922-3.
[19] Hohensinn R, Stauffer R, Pinzon I et al. Low-cost vs. Geodetic-grade GNSS Instrumentation: Geomonitoring with High-rate and Real-time PPP. Proceedings of the 34th International Technical Meeting of the Satellite Division of The Institute of Navigation (ION GNSS+ 2021). 2021. doi: 10.33012/2021.18098.
[20] Takasu T, Yasuda A. Evaluation of RTK-GPS performance with low-cost single-frequency GPS receivers. In: Proceedings of International Symposium on GPS/GNSS; 2008:852–861. Accessed July 15, 2022. https://gpspp.sakura.ne.jp/paper2005/isgps2008_paper_ttaka.pdf.
[21] Odolinski R, Teunissen P. Single-frequency, dual-GNSS versus dual-frequency, single-GNSS: a low-cost and high-grade receivers GPS-BDS RTK analysis. J Geod 2016;90(11):1255–78. https://doi.org/10.1007/s00190-016-0921-x.
[22] Cina A, Piras M. Performance of low-cost GNSS receiver for landslides monitoring: test and results. Geomatics Nat Hazards Risk 2014;6(5–7):497–514. https://doi.org/10.1080/19475705.2014.889046.
[23] Bellone T, Dabove P, Manzino A, Taglioretti C. Real-time monitoring for fast deformations using GNSS low-cost receivers. Geomatics Nat Hazards Risk 2014;7(2):458–70. https://doi.org/10.1080/19475705.2014.966867.
[24] Biagi L, Grec F, Negretti M. Low-Cost GNSS Receivers for Local Monitoring: Experimental Simulation, and Analysis of Displacements. Sensors 2016;16(12):2140. https://doi.org/10.3390/s16122140.
[25] Xue C, Psimoulis P, Zhang Q, Meng X. Analysis of the performance of closely spaced low-cost multi-GNSS receivers. Applied Geomatics 2021;13(3):415–35. https://doi.org/10.1007/s12518-021-00361-8.
[26] Xue C, Psimoulis PA, Meng X. Feasibility analysis of the performance of low-cost GNSS receivers in monitoring dynamic motion. Measurement 2022:111819. https://doi.org/10.1016/j.measurement.2022.111819.
[27] Zhang L, Schwieger V. Investigation regarding different antennas combined with low-cost GPS receivers. Accessed July 15, 2022 In: FIG Working Week FIG 2013. https://www.researchgate.net/publication/350530763_Investigation_Regarding_Different_Antennas_combined_with_Low-Cost_GPS_Receivers.
[28] Jo H, Sim S, Tatkowski A, Spencer B, Nelson M. Feasibility of displacement monitoring using low-cost GPS receivers. Struct Control Health Monit 2012;20(9):1240–54. https://doi.org/10.1002/stc.1532.
[29] Lăpădat A, Tiberius C, Teunissen P. Experimental Evaluation of Smartphone Accelerometer and Low-Cost Dual Frequency GNSS Sensors for Deformation Monitoring. Sensors 2021;21(23):7946. https://doi.org/10.3390/s21237946.
[30] Poluzzi L, Tavasci L, Corsini F, Barbarella M, Gandolfi S. Low-cost GNSS sensors for monitoring applications. Appl Geomatics 2019;12(S1):35–44. https://doi.org/10.1007/s12518-019-00268-5.
[31] Manzini N, Orcesi A, Thom C, et al. Performance analysis of low-cost GNSS stations for structural health monitoring of civil engineering structures. Struct Infrastruct Eng 2020;18(5):595–611. https://doi.org/10.1080/15732479.2020.1849320.
[32] Psimoulis PA, Stiros SC. Measurement of deflections and of oscillation frequencies engineering structures using Robotic Theodolites (RTS). Eng Str 2007;29(12):3312–24. https://doi.org/10.1016/j.engstruct.2007.09.006.
[33] Moschas F, Psimoulis PA, Stiros S. GPS/RTS data fusion to overcome signal deficiencies in certain bridge dynamic monitoring projects, 2013; 12(3–4); 251–69.
[34] Zhang L, Schwieger V. Improving the Quality of Low-Cost GPS Receiver Data for Monitoring Using Spatial Correlations. J Appl Geod 2016;10(2). https://doi.org/10.1515/jag-2015-0022.
[35] Peppa I, Psimoulis P, Meng X. Using the signal-to-noise ratio of GPS records to detect motion of structures. Struct Control Health Monit 2017;25(2):e2080.
[36] Psimoulis P, Peppa I, Bonenberg L, Ince S, Meng X. Combination of GPS and RTS measurements for the monitoring of semi-static and dynamic motion of pedestrian bridge. In: Proceedings of 4th Joint International Symposium of Deformation Monitoring. FIG; 2016. Accessed July 15, 2022. http://www.fig.net/resources/proceedings/2016/2016_03_jisdm_pdf/reviewed/JISDM_2016_submission_103.pdf.
[37] Psimoulis PA, Stiros SC. Measuring deflections of a short-span railway bridge using a robotic total station. J Br Eng 2013;18(2):182–5.
[38] Stiros SC, Psimoulis PA. Response of a historical short-span railway bridge to passing trains: 3-D deflections and dominant frequencies derived from Robotic Total Station (RTS) measurements. Eng Str 2012;2012(45):362–71. https://doi.org/10.1016/j.engstruct.2012.06.029.
[39] Koo KY, Brownjohn JMW, List DI, Cole R. Structural health monitoring of the Tamar suspension bridge. Str Cont Heal Mon 2013;20(4):609–25. https://doi.org/10.1002/stc.1481.
[40] Lienhart W, Ehrhart M, Grick M. High frequent total station measurement for the monitoring of bridge vibrations. J Appl Geod 2017;11(1):1–8. https://doi.org/10.1515/jag-2016-0028.
[41] Meo M, Zumpano G, Meng X, Cosser E, Roberts G, Dodson A. Measurements of dynamic properties of a medium span suspension bridge by using the wavelet transforms. Mech Syst Signal Process 2006;20(5):1112–33. https://doi.org/10.1016/j.ymssp.2004.09.008.
[42] Vishvaksenan KS, Mithra K, Kalaiarasan R, Raj KS. Mutual Coupling Reduction in Microstrip Patch Antenna Arrays Using Parallel Coupled-Line Resonators. IEEE Antennas Wirel Propag Lett 2017;16:2146–9. https://doi.org/10.1109/lawp.2017.2700521.
[43] Leica Geosystems AG. Leica Viva GS10 Data Sheet. 2015. Accessed July 15, 2022. https://leica-geosystems.com/-/media/files/leicageosystems/products/datasheets/leica_viva_gs10_ds.ashx?la=en&hash=8235B2E48B48F7A09895BA20C1033B58.
[44] U-blox AG. NEO/LEA-M8T U-Blox M8 Concurrent GNSS Timing Modules Data Sheet. 2020. Accessed July 15, 2022. https://www.u-blox.com/sites/default/files/NEO-LEA-M8T-FW3_DataSheet_%28UBX-15025193%29.pdf.
[45] Leica Geosystems AG. Leica Nova MS60 MultiStation: Master Your Projects. 2020. Accessed July 15, 2022. https://leica-geosystems.com/-/media/files/leicageosystems/products/datasheets/leica_nova_ms60_ds.ashx?la=en&hash=AB5679E327538292C23BD76C0CCF3B52.
[46] Everett T. RTKLIB Code: Windows executables. rtkexplorer. Published October 20, 2016. Accessed July 15, 2022. http://rtkexplorer.com/downloads/rtklib-code/.
[47] Takasu T, Yasuda A. Development of the low-cost RTK-GPS receiver with an open source program package RTKLIB. In: International Symposium on GPS/GNSS. Vol 1; 2009. Accessed July 15, 2022. https://gpspp.sakura.ne.jp/paper2005/isgps_2009_rklib.pdf.
[48] Everett T. Documentation of differences between RTKLIB demo5 and RTKLIB 2.4.3. rtkexplorer. Published November 12, 2016. Accessed July 15, 2022. http://rtkexplorer.com/downloads/rtklib-code/documentation-of-differences-between-rtklib-demo5-and-rtklib-2-4-3/.

[49] Everett T. Glonass Ambiguity Resolution with RTKLIB Revisited. rtklibexplorer. Published June 14, 2018. Accessed July 15, 2022. https://rtklibexplorer.wordpress.com/2018/06/14/glonass-ambiguity-resolution-with-rtklib-revisited/.
[50] Choi K, Bilich A, Larson K, Axelrad P. Modified sidereal filtering: Implications for high-rate GPS positioning. Geophys Res Lett 2004;31(22). https://doi.org/10.1029/2004gl021621.
[51] Benton C, Mitchell C. Isolating the multipath component in GNSS signal-to-noise data and locating reflecting objects. Radio Sci 2011;46(6). https://doi.org/10.1029/2011rs004767.
[52] Ogaja C, Satirapod C. Analysis of high-frequency multipath in 1-Hz GPS kinematic solutions. GPS Solutions 2007;11(4):269–80. https://doi.org/10.1007/s10291-007-0058-8.
[53] Rothacher M, Schaer S, Mervart L, Beutler G. Determination of antenna phase center variations using GPS data. IGS Workshop Proceedings: Special Topics and New Directions. 1995; 205–20.
[54] Li X, Ge M, Dai X, et al. Accuracy and reliability of multi-GNSS real-time precise positioning: GPS, GLONASS, BeiDou, and Galileo. J Geod 2015;89(6):607–35. https://doi.org/10.1007/s00190-015-0802-8.
[55] Msaewe H, Hancock C, Psimoulis P, Roberts G, Bonenberg L, de Ligt H. Investigating multi-GNSS performance in the UK and China based on a zero-baseline measurement approach. Measurement 2017;102:186–99. https://doi.org/10.1016/j.measurement.2017.02.004.
[56] Psimoulis P, Houlié N, Behr Y. Real-Time Magnitude Characterization of Large Earthquakes Using the Predominant Period Derived From 1 Hz GPS Data. Geophys Res Lett 2018;45(2):517–26. https://doi.org/10.1002/2017gl075816.
[57] Moschas F, Stiros SC. Three-dimensional dynamic deflections and natural frequencies of a stiff footbridge based on measurements of collocated sensors. Str Cont Heal Mon 2014;21:23–42.
[58] Hohensinn R, Stauffer R, Glaner MF, et al. Low-cost GNSS and real-time PPP: Assessing the precision of the u-blox ZED-F9P for kinematic monitoring application. Rem Sen 2022;14(20):5100. https://doi.org/10.3390/rs14205100.